ELSEVIER

Journal of Alloys and Compounds 320 (2001) 251–261

Journal of ALLOYS AND COMPOUNDS

www.elsevier.com/locate/jallcom

# Phase equilibria and thermal analysis of Si–C–N ceramics

Hans Jürgen Seifert*, Jianqiang Peng, Hans Leo Lukas, Fritz Aldinger

*Max-Planck-Institut für Metallforschung and Institut für Nichtmetallische Anorganische Materialien, Universität Stuttgart, Pulvermetallurgisches Laboratorium, Heisenbergstr. 5, 70569 Stuttgart, Germany*

**Abstract**

The phase reactions, crystallization behaviour and thermal degradation of two Si–C–N ceramics derived from precursors VT50 and NCP200, respectively, were studied by means of CALPHAD type thermodynamic calculations and experimental investigations by DTA/TG, XRD and SEM/EDX. The phase reaction $Si_3N_4+3C=3SiC+2N_2$ proceeds during the thermal degradation of both ceramics. Additionally, the phase reaction $Si_3N_4=3Si+2N_2$ occurs during the thermal degradation of the NCP200 ceramic. To explain quantitatively the high temperature behaviour of Si–C–N ceramics, thermodynamic functions, the reaction scheme, isothermal sections, isopleths, phase fraction diagrams and phase composition diagrams (for gas partial pressures) were calculated. The computer simulations were confirmed by the experiments for both ceramics. 

*Keywords:* Si–C–N ceramics; CALPHAD; Thermodynamics; Thermal analysis

## 1. Introduction

Ceramics based on non-oxide compounds such as $Si_3N_4$ and SiC are suitable candidates for high temperature applications. SiC-reinforced $Si_3N_4$ composites are fabricated by addition of whiskers, fibres or platelets of SiC to $Si_3N_4$. Such materials are conventionally prepared by powder technology using sintering additives (e.g. $Y_2O_3$, $Al_2O_3$) or nitriding a Si–SiC compact at high temperatures. To predict and control the sintering conditions (temperature, pressure, composition of samples and atmosphere) for such materials numerous thermochemical analyses of phase equilibria in the Si–C–N system have been published [1–10]. Most of these publications take into account the influence of the nitrogen partial pressure and the activity of carbon on phase equilibria. The results provided guidelines for the developing of such materials. The present paper considers most recent thermodynamic data for the Si–C–N system which are used for the calculation of phase equilibria and phase reactions in precursor-derived Si–C–N ceramics.

The use of precursors has attracted wide attention as an alternative approach to produce $Si_3N_4$–SiC ceramics and offers a number of advantages compared to classic powder technology. With the synthesis of Si–C–N ceramics from precursor polymers one can control the materials composition, structures and properties on an atomic scale [11–16]. Highly homogeneous ceramics may be prepared and shaped without a sintering aid. Furthermore, it can provide processing opportunities for some applications such as coating or fibre preparation. According to this route polysilazane is crosslinked and then pyrolysed into amorphous Si–C–N ceramics with a completely homogeneous distribution of the elements and remaining amorphous up to 1700 K in argon or nitrogen and 1800 K in air [14,15]. At temperatures higher than 1700 K in argon or nitrogen this amorphous state is transformed into polycrystalline ceramics consisting of thermodynamic stable phases, such as $Si_3N_4$, SiC and graphite. Since the pyrolysis products can be used as both amorphous and crystalline materials, the understanding of the high temperature behaviour of the ceramics and the phase reactions, the crystallization behaviour and the accompanied material thermal degradation are of great importance with respect to the physico-chemical properties of the polycrystalline ceramics and to the maximum application temperature of the amorphous ceramics.

To simulate and predict the phase equilibria and phase reactions in ceramics of the Si–C–N system, thermodynamic calculations by the CALPHAD method (CALculation of PHAse Diagram [17]) were carried out. Various types of phase diagrams, phase fraction diagrams, phase composition diagrams and thermodynamic functions were computer calculated using modern software and the most

*Corresponding author. Tel.: +49-711-686-1105; fax: +49-711-686-1131.

*E-mail address:* seifert@aldix.mpi-stuttgart.mpg.de (H.J. Seifert).

0925-8388/01/$ – see front matter 
PII: S0925-8388(00)01478-X

reliable thermodynamic data for the Si–C–N system. This information can be used for temperatures higher than about 1700 K where the materials start to crystallize [18–20]. At lower temperatures precursor-derived samples may remain even after long-term heat treatment in a nonequilibrium state (amorphous, partially crystalline) where the phase configuration cannot be reproduced by equilibrium calculations.

The computer simulations were confirmed by experimental investigations using thermal analysis, X-ray diffractometry and microscopic methods.

## 2. Thermodynamic calculations

The CALPHAD method [17] was used to simulate and understand phase reactions and crystallization behaviour of precursor-derived ceramics. The diagrams were calculated using the software of Lukas [21] and ThermoCalc [22]. The thermodynamic data for the binary systems Si–C and Si–N used in this work were taken from Refs. [23,24], respectively. The assessment of these systems is based on data for the pure elements Si, C and N provided by Dinsdale [25] and stored in the SGTE database [26]. The data for gaseous species $N_2$, Si, $Si_2$, $Si_2C$, $SiC_2$, CN and $C_2N_2$ and some others were taken from the SGTE substance database [26]. Beside the gas phase, the liquid phase and the solid phases, silicon, graphite, $Si_3N_4$ and SiC were taken into account. β-$Si_3N_4$ is the stable modification of the compound $Si_3N_4$ whereas α-$Si_3N_4$ is a metastable modification [27]. A single analytical Gibbs-energy description was used to describe α- and β-SiC. The ternary phases $SiC_2N_4$ and $Si_2CN_4$ documented by Riedel et al. [28], are reported not to be stable at conditions treated here ($p = 1$ bar, $T > 1300$ K). The postulated compound $C_3N_4$ [29] was not found as solid phase until now.

More recent discussions on the experimental information on the thermodynamics of α- and β-SiC were provided recently by Kleykamp [30] and α- and β-$Si_3N_4$ by Liang et al. [27] and O'Hare et al. [31]. These publications confirm the analytical descriptions used in the present work.

The phase reactions in the ternary system Si–C–N can be simulated by extrapolating calculations since all solid phases have negligible ranges of solubility. To simulate and predict the phase reactions of precursor-derived ceramics, thermodynamic functions, the reaction scheme, isothermal sections, isopleths, phase fraction diagrams and phase composition diagrams (for gas partial pressures) were calculated.

## 3. Experimental procedure

Amorphous Si–C–N ceramics were derived from commercially available precursors VT50 (polyvinylsilazane (PVS); Hoechst AG, Frankfurt, Germany) with composition $Si_1C_{1.6}N_{1.33}$ (25.4 Si, 40.7 C, 33.8 N; at.%) and NCP200 (polyhydridomethylsilazane (PHMS); Nichimen Corp., Tokyo, Japan) with composition $Si_1C_{0.6}N_{1.02}$ (38.2 Si, 22.9 C, 38.9 N; at.%), as described in detail elsewhere [32,33]. The polysilazanes were crosslinked at temperatures between 473 and 673 K under vacuum and in Ar atmosphere, and then thermolysed at a temperature of 1323 K under Ar atmosphere into the amorphous ceramics. The amorphous ceramics were milled for 20 min using WC balls. The mean particle size of the resulting powder was measured by laser scattering (Granulometer HR 850, Cilas-Alcatel). An average value of about 10 μm was found. The content of oxygen in both amorphous ceramics was less than 1 mass% measured by carrier gas hot extraction with thermal conductivity and infrared absorption detectors (TC 436, Leco).

Investigations by differential thermal analysis (DTA) and thermogravimetry (TG) were carried out simultaneously in BN crucibles (Simultaneous Thermal Analysis, STA; Bähr STA501 with graphite heating element). Flowing nitrogen atmosphere (Messer-Griesheim; nitrogen 5.0, oxygen $<$ 5 vpm, flowing rate: 2 l/h) was used. The heating rate was 10 K/min up to 1273 K, and 5 K/min up to the maximum temperature of 2073 or 2273 K.

The phase configuration was analysed by X-ray diffractometry (XRD; Siemens Diffraktometer D5000/Kristalloflex, Cu $K\alpha_1$ radiation). Microstructures and phase compositions were investigated by scanning electron microscopy (SEM; Zeiss DSM982 GEMINI) coupled with energy dispersive X-ray spectroscopy (EDX; Oxford-Instrument ISIS 300).

## 4. Results and discussion

### 4.1. Thermodynamic calculations

Fig. 1 shows calculated isothermal, isobaric ($p = 1$ bar) sections in the ternary system Si–C–N for the temperatures 1687 K $< T <$ 1757 K (Fig. 1a), 1757 K $< T <$ 2114 K (Fig. 1b), $T = 2123$ K (Fig. 1c) and $T = 3000$ K (Fig. 1d). Below a temperature of 1687 K silicon exists as solid phase. From the experimental point of view nitrogen escapes at 1 bar, but for the calculation it is in the gas phase and still part of the system (included in the mole fraction). The phase equilibria, compositions of the asthermolysed amorphous ceramics made from VT50- or NCP200-precursors and correlated reaction paths are indicated (arrows in Fig. 1b and c, respectively). The reaction paths [34] indicate the change of the gross composition of the solid samples due to the loss of nitrogen according to the nonvariant reactions

$$Si_3N_4\,(s) + 3C\,(s) = 3SiC\,(s) + 2N_2\,(g);\ T = 1757\ K \qquad (1)$$

and

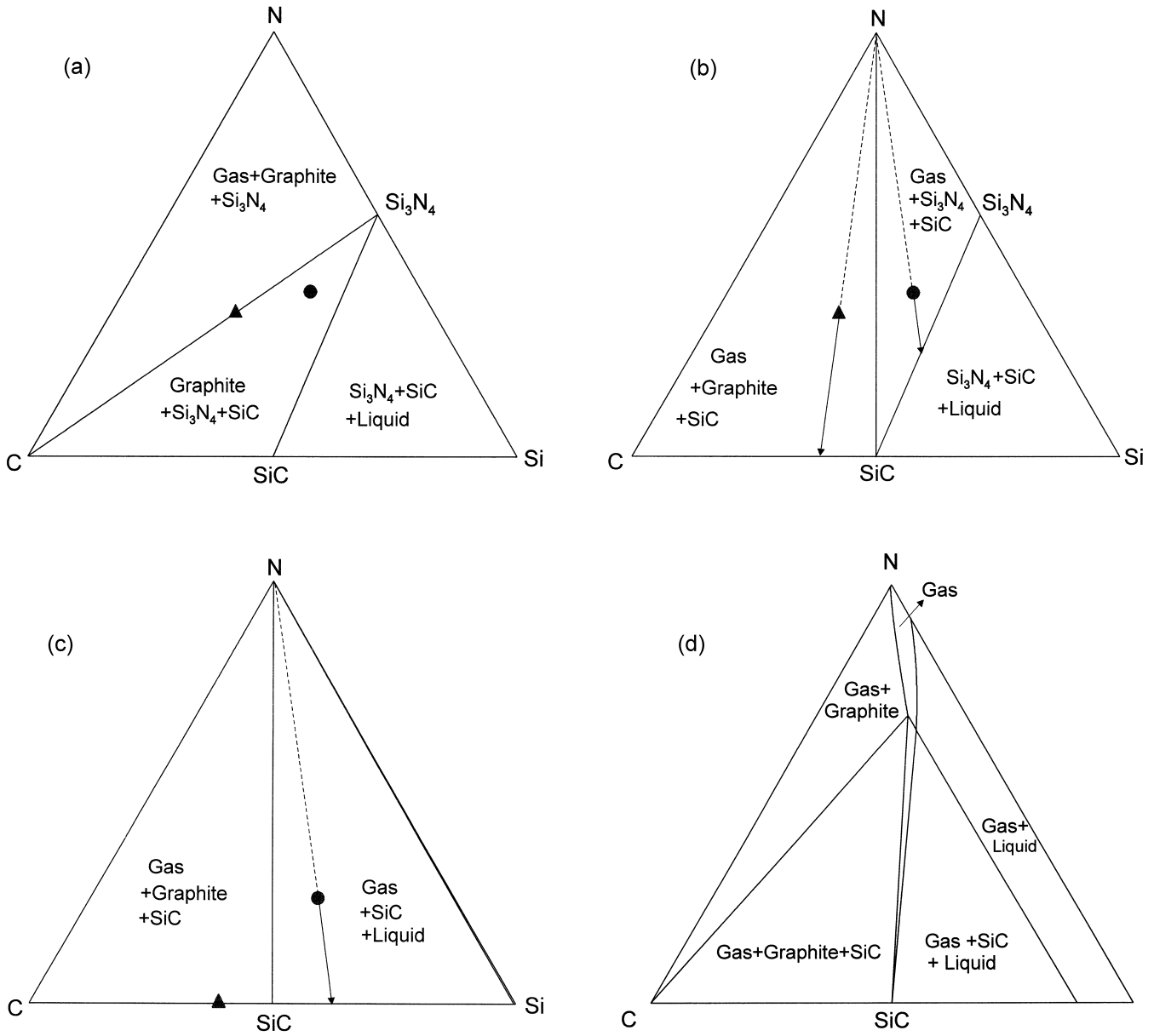


Fig. 1. Isothermal, isobaric sections in the Si–C–N system at 1 bar. The compositions of the amorphous VT50- and NCP200-derived ceramics (▲, ●) and reaction paths (arrows) are indicated. (a) 1687 K$<T<$1757 K; (b) 1757 K$<T<$2114 K; (c) $T = 2123$ K; (d) $T = 3000$ K.

$$Si_3N_4\ (s) = 3Si\ (l) + 2N_2\ (g);\ T = 2114\ K \quad (2)$$

In connection with reaction (1) the VT50 ceramic with a ratio C:Si$>$1 produces nitrogen until the indicated reaction path ends on the tie line graphite–SiC (Fig. 1b) whereas the ceramic NCP200 with a ratio C:Si$<$1 produces nitrogen and changes the composition to the SiC–$Si_3N_4$ tie line. At temperatures above 2114 K the NCP200-derived ceramic again loses nitrogen (Fig. 1c) because the residual $Si_3N_4$ dissociates into liquid silicon and nitrogen gas according to reaction (2).

Fig. 1d shows the calculated isothermal section in the Si–C–N system at a temperature of 3000 K. At such high temperatures liquid silicon dissolves some carbon and the ternary gas phase region is significantly extended. The gas phase does not only consist of $N_2$ but as well of other gaseous species such as Si, $Si_2$, $SiC_2$, $Si_2C$, CN and $C_2N_2$ as given in Fig. 2 which shows the partial pressures of different gaseous species concerning the gas phase related to the VT50-derived ceramic at a total pressure of 1 bar. Fig. 3a shows two dashed lines within the isothermal section valid at temperatures between 1757 and 2114 K (Fig. 1b) which are the composition lines of two isopleths shown in Fig. 3b and c (C–42.9 Si, 57.1 N; C–49.5 Si, 50.5 N; at.%) including the compositions of the VT50- and NCP200-derived ceramics. At temperatures below 1757 K both materials consist of graphite, $Si_3N_4$ and SiC. At higher temperatures the compositions without gas are

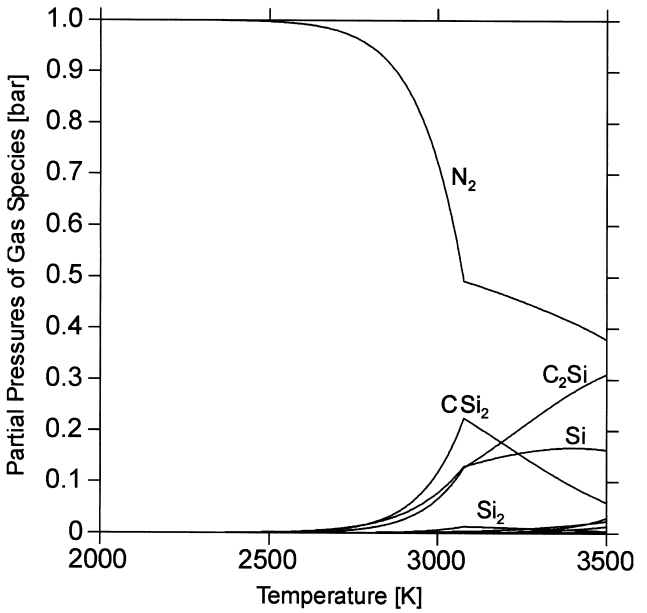


Fig. 2. Partial pressures for the gas phase in equilibrium with VT50-derived ceramics.

located outside the indicated composition lines of the isopleths (see reactions paths in Fig. 1b). In accordance with the isothermal section at $T > 1757$ K the condensed materials consist of graphite and SiC (VT50) or $Si_3N_4$ and SiC (NCP200), respectively.

Based on these calculations the Scheil-reaction scheme [35] for the Si–C–N system (valid for $p = 1$ bar) was derived (Fig. 4). The scheme is similar to the one presented by Weiss et al. [3] but with improved reaction temperatures. The reactions (1) and (2) are indicated as $U_2$ and $p_2$, respectively. The melting point of Si is indicated by reaction $D_2$. Because of lack of data the transformation β-SiC/α-SiC was not taken into account. The α-$Si_3N_4$/β-$Si_3N_4$ transformation was not taken into account as α-$Si_3N_4$ is assumed to be a metastable phase [27] (see Section 2).

The influence of the gas phase on the phase reactions is shown in Fig. 5 by the calculated potential phase diagrams for C:Si>1 (Fig. 5a, valid for e.g. VT50 ceramic) and C:Si<1 (Fig. 5b, valid for e.g. NCP200 ceramic). The method of calculation of such diagrams is described elsewhere [36]. Here the gas phase is considered to be outside the system, but may exchange nitrogen with the system. Along the line identical in both figures the three phases, graphite, SiC and $Si_3N_4$ are in equilibrium and show the reaction (1). Below the line either the two-phase field SiC+C (C:Si>1) or SiC+$Si_3N_4$ (C:Si<1) exists. $Si_3N_4$ decomposes at low partial pressures of $N_2$ according to reaction (2) into nitrogen and liquid or solid Si which is in equilibrium with SiC. Note the change of the reaction temperatures with the changing partial pressure of nitrogen. The reaction temperatures given in the Scheil reaction scheme (Fig. 4) are valid for a total pressure of 1 bar. The diagrams give advice for the sintering of $Si_3N_4$–SiC samples. If the $N_2$-partial pressure is above the line SiC+C+$Si_3N_4$ the sample is stable at the sintering temperature. For sintering of SiC+$Si_3N_4$ there are temperature-dependent upper and lower limits for the $N_2$-pressure for the stability range. For more details see Refs. [5,8,36].

Additionally, quantitative mass balances and the enthalpies of phase reactions can be calculated for the ceramics which appear in the experimental STA investigations. For this purpose phase fraction diagrams were calculated. Fig. 6a shows this type of diagram calculated for a total pressure of 1 bar for the composition of VT50-derived ceramic (C:Si>1) where at the aforementioned temperature of 1757 K according to reaction (1) 70.7 mass% $Si_3N_4$, 29.2 mass% graphite and negligible amount of SiC form 60.7 mass% of SiC and 28.3 mass% of nitrogen. The predicted sample mass loss due to nitrogen evolution is 28.3%. The gas phase in calculation still belongs to the system but appears as 'mass loss' in TG experiments; 11 mass% excess graphite remain. In VT50-derived ceramics no $Si_3N_4$ is found any longer. The changing composition with the different gaseous species constituting the gas phase at different temperatures is shown in the calculated diagram of Fig. 2.

For NCP200-derived ceramic (Fig. 6b) with a ratio C:Si<1 all carbon is consumed and there is a mass loss of 13.7% due to reaction (1). After the reaction excess $Si_3N_4$ remains. At temperatures higher than 1841°C (2114 K) this residual $Si_3N_4$ decomposes according to reaction (2) causing a further mass loss of 15.1%. The balanced reaction Eq. (1) is only valid for a ratio C:$Si_3N_4$ defined by the intersection of the inner tie-lines C–$Si_3N_4$ and N–SiC of the four phase reaction (1) (79.6 mass% $Si_3N_4$, 20.4 mass% graphite). For precursor ceramics with lower carbon content (e.g. NCP200) all carbon is consumed during reaction (2) and $Si_3N_4$ remains.

The length of the arrows indicating the reaction paths in Fig. 1b and c gives the value of the relative change of the nitrogen content of the solid samples. In the case of VT50-derived ceramic a direct comparison with the result of the calculated phase fraction diagram is possible. The composition of this ceramic changes according to the sequence $Si_1C_{1.6}N_{1.33}$ (25.4 Si, 40.7 C, 33.8 N; at.%)→$Si_1C_{1.6}$ (38.5 Si, 61.5 C; at.%). The final solid sample lost the complete nitrogen content of 33.8 at.%. This value can be found from the indicated reaction path (arrow) for VT50-derived ceramics in Fig. 1b and corresponds to the 28.3 mass% calculated in the phase fraction diagram (Fig. 6a). The relationship between the reaction paths and the calculated phase fraction diagram for the NCP200-derived ceramic is not as obvious as for the VT50-derived ceramics. The composition of that ceramic changes during the reactions (1) and (2) according to the following sequence:

(a) $(Si_1C_{0.6})N_{1.02}$ (38.2 Si, 22.9 C, 38.9 N; at.%) →
$(Si_1C_{0.6})N_{0.53}$ (46.9 Si, 28.1 C, 25 N; at.%)

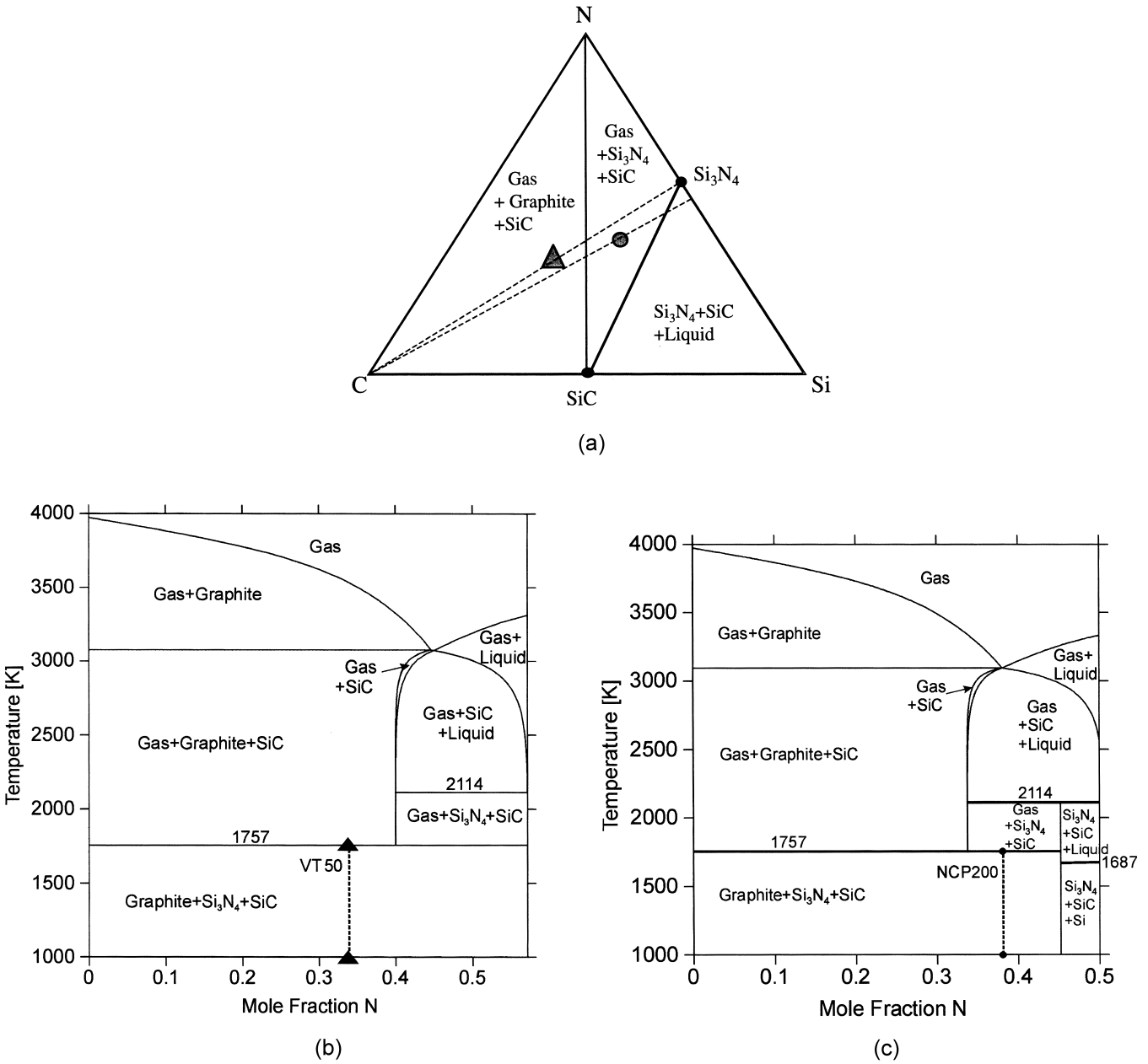


Fig. 3. Isopleths in the Si–C–N system. Compositions of VT50- and NCP200-derived ceramics are indicated. (a) Isothermal section for temperature range 1757 K$<T<$2114 K with indicated composition lines of isopleths shown in (b) and (c). (b) Isopleth C–42.9 Si, 57.1 N (at.%). (c) Isopleth C–49.5 Si, 50.5 N (at.%).

(b) $(Si_1C_{0.6})N_{0.53}$ (46.9 Si, 28.1 C, 25 N; at.%) →

$Si_1C_{0.6}$ (62.5 Si, 37.5 C; at.%).

The length of the corresponding two arrows (reaction paths in Fig. 1b and c, respectively) give only the relative change of the nitrogen content of the solid samples. After the first step (a) the nitrogen content of the solid sample is 25 at.%. The phase fraction diagram gives a mass loss of 13.7% which corresponds to 18.5 at.%. At first glance this value does not agree with the value of nitrogen loss derived from the length of the arrow in Fig. 1b which is 13.9 at.%. The data of the phase fraction diagram calculation refer to the total system including the gas phase which released during the reaction at 1757 K, whereas the 25 at.% are referred to the solid residue after this reaction. The calculation assumes the gas phase always as part of the system as described in Section 4.1. On the other hand the data from the indicated reaction paths refer only to the composition of the solid phases without taking into account the released gas phase. The calculated mass loss of the second step is 15.1 mass% (20.4 at.%) of the initial sample or 25.0 at.% referred to the residue of step 1.

Fig. 6a and b show that at temperatures higher than 2600

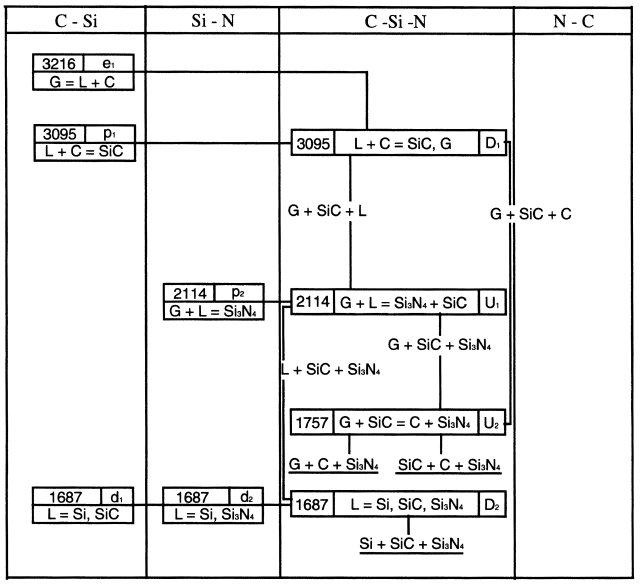


Fig. 4. Scheil reaction scheme for the Si–C–N system (β-SiC/α-SiC and $\alpha$-$Si_3N_4$/$\beta$-$Si_3N_4$ transformations not indicated).

K the SiC fraction decreases whereas the fraction of the gas phase increases. This results from the formation of the gaseous species $CSi_2$ and $C_2Si$ at such high temperatures as shown for the composition of the VT50-derived ceramic in Fig. 2.

The DTA experiments can be simulated by calculating enthalpy–temperature diagrams (Fig. 7). The calculated enthalpy–temperature diagram shows for VT50-derived ceramic an endothermic heat effect of +52.3 kJ/mol (moles of atoms of total sample) for reaction (1). Only part of the sample is involved in the reaction and therefore the heat effect is lower than expected for a ratio of phases sufficient for complete reaction. The enthalpy of reaction (1) in NCP200-derived ceramic is +28.5 kJ/mol and of reaction (2) it is +49.5 kJ/mol.

It has to be decided which crucible material is suitable for the heat treatment and thermal analyses of the ceramic samples, i.e. it must not react with the sample. Graphite crucibles are not adequate because they react with $Si_3N_4$. An alternative crucible material is BN. The reaction of VT50-derived ceramics of composition $Si_1C_{1.6}N_{1.33}$ with BN was simulated. The result is shown as phase fraction diagram in Fig. 8. The calculation shows that BN does not take part in reaction (1) (i.e. $U_2$ in Fig. 4). According to the equilibrium calculation BN is formed at temperatures lower than 1000 K and remains inert until the reaction of BN with SiC at the temperature of 2586 K. Based on this result, BN crucibles were used for thermal analyses.

### *4.2. Experimental investigations*

Fig. 9a and b show the DTA/TG curves for the VT50-derived and the NCP200-derived ceramic, respectively.

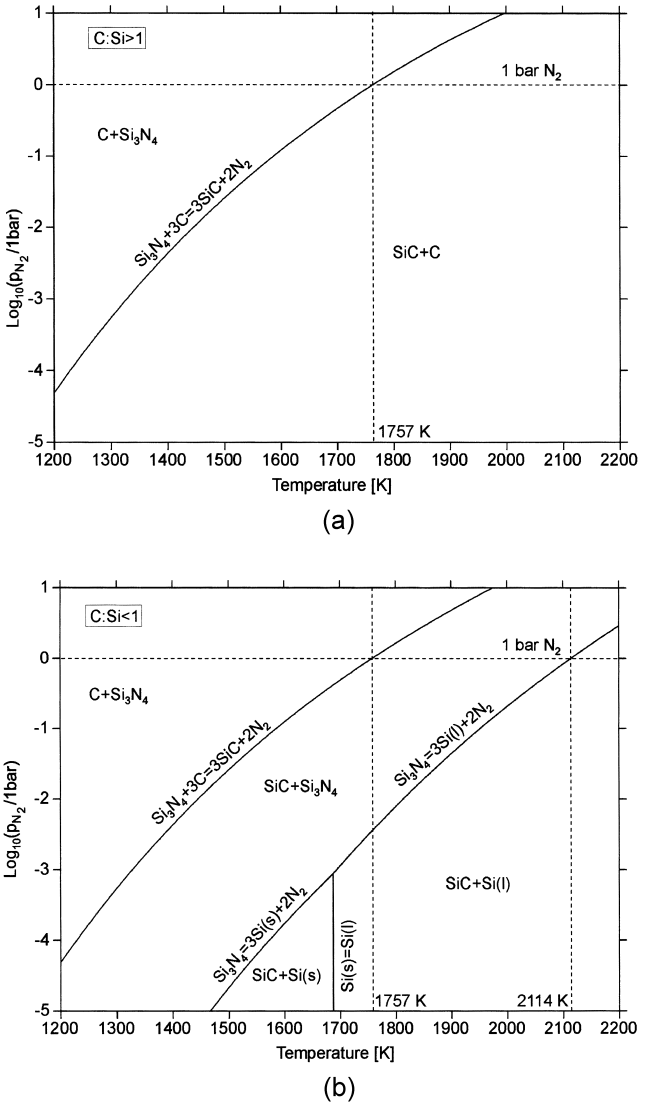


Fig. 5. Potential phase diagrams for the Si–C–N system [36]. (a) C:Si> 1; (b) C:Si<1.

The TG analysis of VT50 ceramic shows a mass loss of 29% between 1600°C (1873 K) and 1690°C (1963 K). Simultaneously an endothermic reaction peak was found by DTA. This mass loss and endothermic reaction peak can be explained by reaction (1) (Figs. 1a,b and 6a) although the reaction temperature is higher than the calculated one (1757 K).

This shift of the measured reaction temperature for reaction (1) can be explained by kinetic hindrance. As shown by Bill et al. [37] an extended heat treatment of VT50 precursor-derived ceramic is necessary to completely crystallize the material at 1773 K and find the equilibrium phases. After heat treatment for 50 h at 1773 K in nitrogen atmosphere the material consists only of SiC and carbon. This result confirms that reaction (1) occurs close to the calculated reaction temperature of 1757 K. However, because of the sluggishness of the reaction its temperature

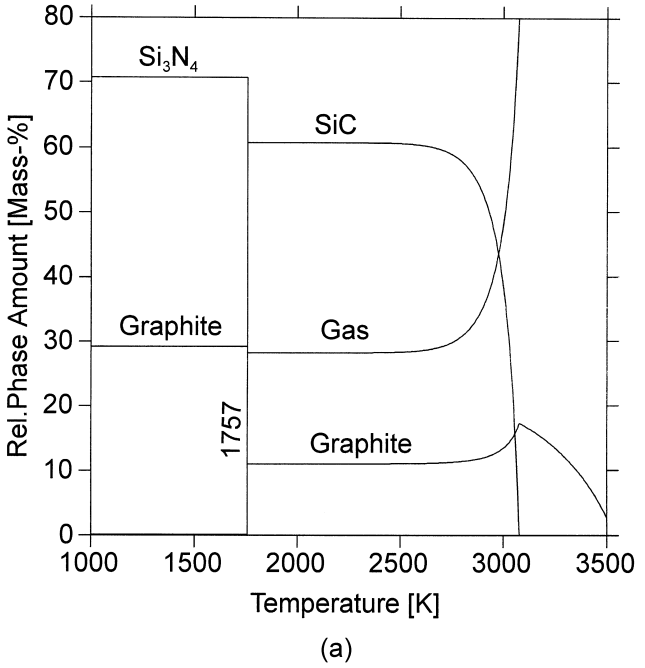


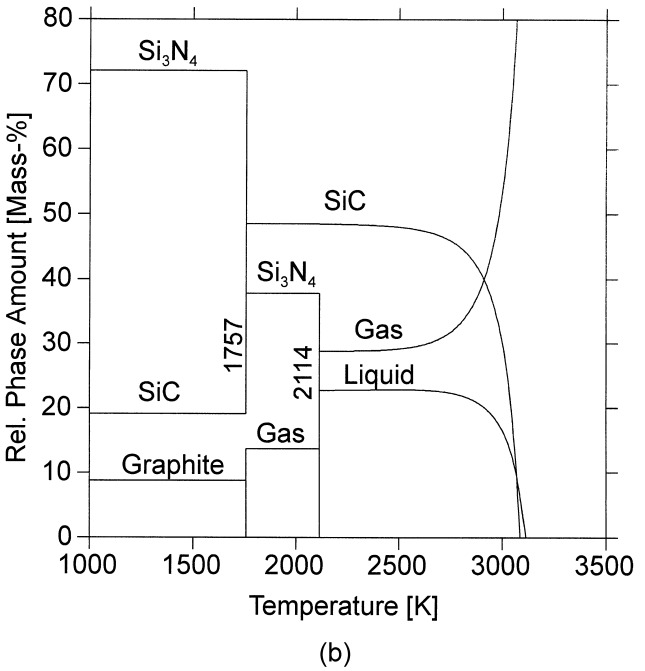


Fig. 6. Calculated phase fraction diagrams in the Si–C–N system. (a) VT50-derived ceramics (C:Si>1). (b) NCP200-derived ceramics (C:Si< 1).

cannot be detected exactly by thermal analysis using a defined heating rate (this work: 5 K/min, see Section 3).

The influence of the small oxygen amount in the samples (<1 mass%) on the reaction behavior is negligible. No (protective) $SiO_2$ layers were found by transmission electron microscopy [37] in VT50 precursor-derived ceramics. Additionally, the oxygen fraction in the flowing

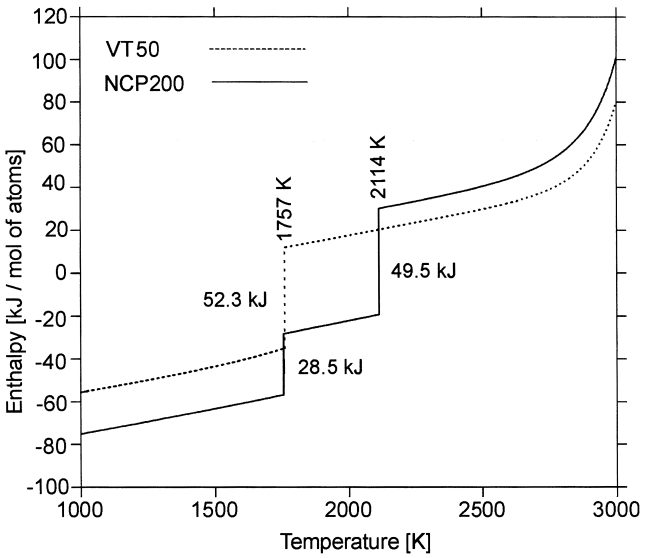


Fig. 7. Calculated enthalpy–temperature diagram for the VT50- and NCP200-derived ceramics.

$N_2$-atmosphere is very small (see Section 3) and immediately reacts with the graphite heating elements used.

In the case of NCP200 ceramic, the two steps of mass loss with accompanied endothermic reactions could be detected as predicted by thermodynamic calculation (Figs. 1a,b and 6b). In the temperature range from 1600°C (1873 K) to 1690°C (1963 K) 12% mass loss and an endothermic reaction peak was detected, and between 1840°C (2113 K) and 1900°C (2173 K) 15% mass loss and an endothermic reaction peak was determined. The first endothermic peak

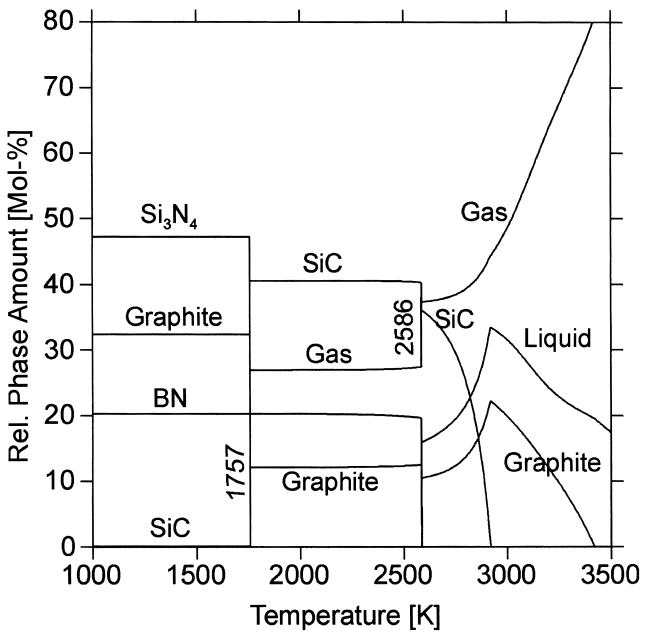


Fig. 8. Phase fraction diagram for the combination of VT50-derived ceramic with BN.

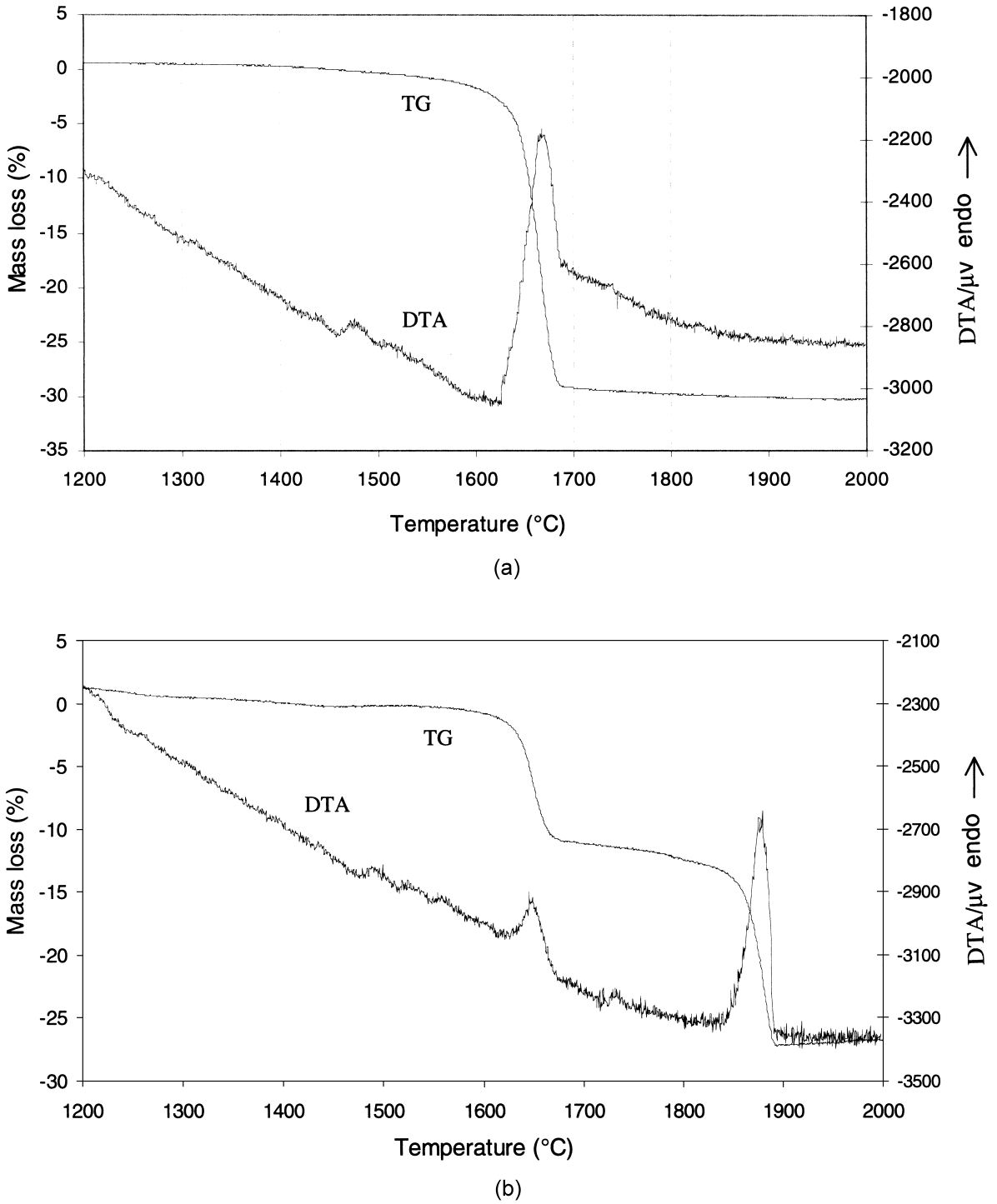


Fig. 9. DTA/TG measurements (STA) for precursor-derived ceramics; $N_2$ atmosphere, BN-crucible, 10 K/min up to 1000°C (1273 K), 5 K/min up to 2000°C (2273 K). (a) VT50-derived ceramics; (b) NCP200-derived ceramics.

can be attributed to reaction (1), although this temperature is higher than calculated for reasons similar as discussed for VT50-derived ceramics. The second endothermic peak is due to the decomposition of residual $Si_3N_4$ according to reaction (2). The two steps of mass loss agree quantitatively with the calculated ones.

The ratio of the three experimentally derived enthalpy values (the area of the endothermic peaks) is similar to the ratio of the calculated enthalpies (Fig. 9). The temperature of reaction (2) is in agreement with the calculated one.

XRD and SEM combined with EDX were used to confirm the results obtained by STA and the thermodynamic calculations. Fig. 10 shows the XRD patterns of the VT50-derived ceramic. The structure of this material

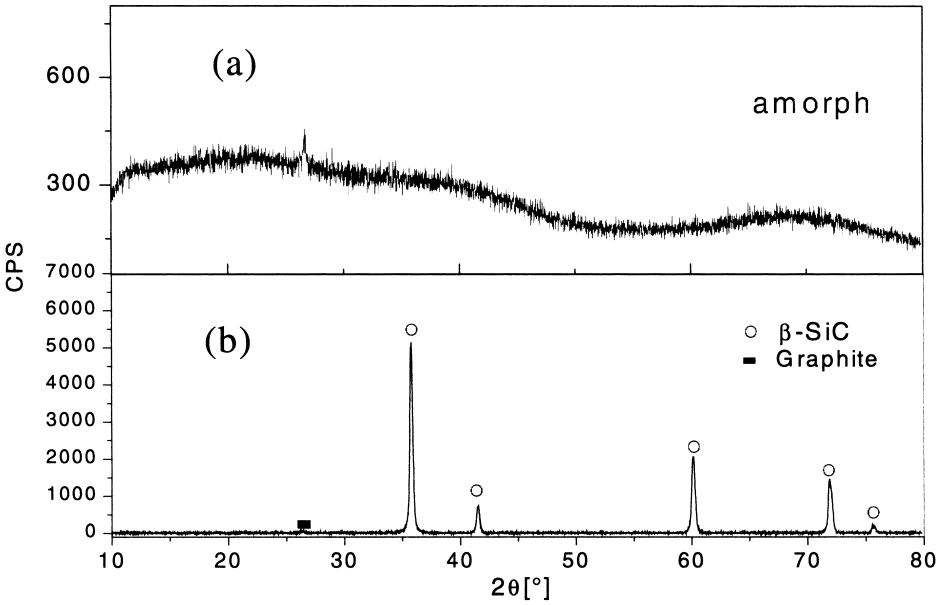


Fig. 10. XRD patterns of the VT50-derived ceramic. (a) Before STA. (b) After STA up to 2000°C (2273 K).

before STA is almost completely amorphous as shown in Fig. 10a. After STA with upper temperature of 2000°C (2273 K, Fig. 9a) the material consists of crystalline β-SiC and graphite (Fig. 10b), which is in accordance with the calculations (Figs. 1a,b and 6a). In case of the NCP200-derived ceramic, after STA up to 1800°C (2073 K, Fig. 9b)

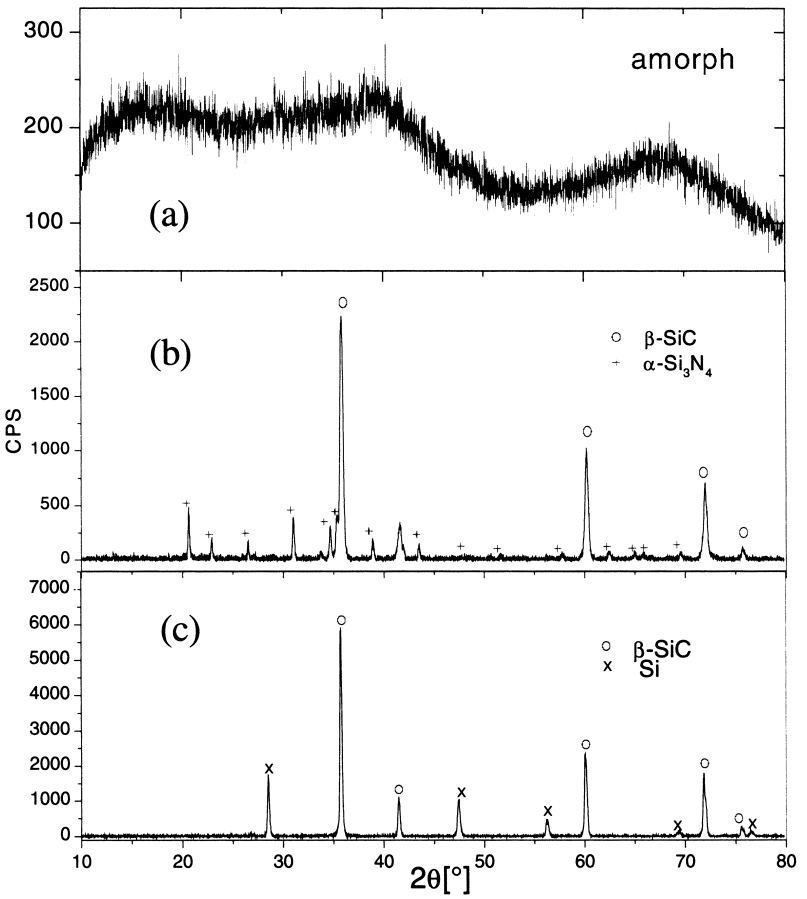


Fig. 11. XRD pattern of the NCP200-derived ceramic. (a) Before STA. (b) After STA up to 1800°C (2073 K). (c) After STA up to 2000°C (2273 K).

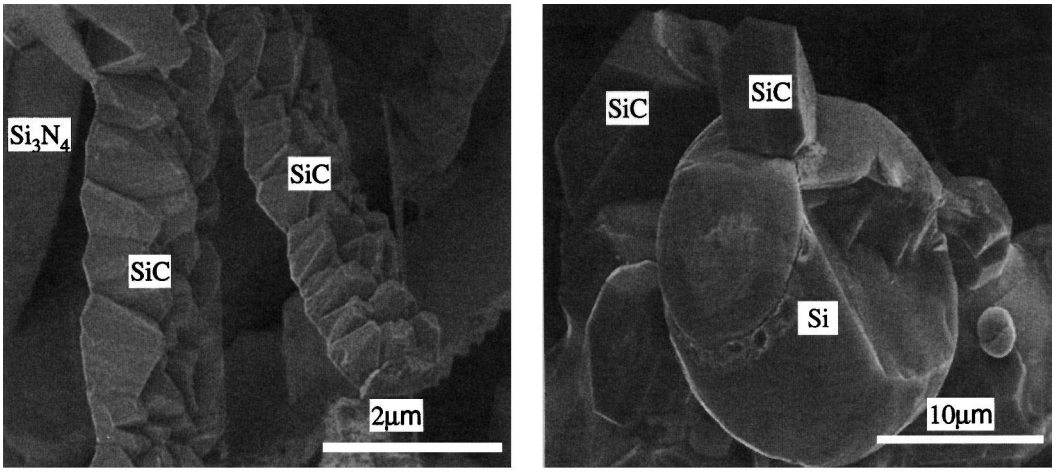


Fig. 12. SEM images of NCP200-derived ceramics. (a) After STA up to 1800°C (2073 K). (b) After STA up to 2000°C (2273 K).

the phase configuration changes to β-SiC/α-$Si_3N_4$ or to β-SiC/Si, if the STA is continued up to 2000°C (2273 K, Fig. 9b). Comparing the XRD patterns of the NCP200-derived ceramics in Fig. 11a–c with Figs. 1a–c and 6b shows that the experimental results are also correctly simulated by the calculation.

Fig. 12 shows SEM images of NCP200-derived ceramic. Heating up to 1800°C (2073 K, Fig. 12a) clearly β-SiC/$Si_3N_4$ can be recognized, whereas after heating up to 2000°C (2273 K, Fig. 12b) besides β-SiC silicon can be seen which has still the shape of solidified droplets. The phase compositions were confirmed by EDX analyses.

## 5. Conclusion

The results of the experimental investigation of VT50- and NCP200-derived ceramics show that CALPHAD-type simulations can quantitatively predict their high-temperature behaviour. The present work shows that thermodynamic calculations can be used successfully to support the development of Si–C–N ceramics using the powder technology and the precursor route, respectively. From these calculations the phase equilibria, phase compositions, phase reactions and the accompanied microstructure development can be derived. Such information provides guidelines for favourable sintering and processing conditions and the understanding of the materials reactions during application. Additionally, kinetic effects (e.g. during crystallization of amorphous ceramics) and the formation of metastable phases (e.g. α-$Si_3N_4$) have to be taken into account.

## Acknowledgements

We thank the Deutsche Forschungsgemeinschaft (DFG) and the Japan Science and Technology Corporation (JST) for financial support. For providing samples we are grateful to J. Bill, P. Gerstel, S. Prinz and J. Seitz. The authors thank M. Thomas, H. Kummer and H. Labitzke for support in experimental analyses.

## References

[1] H. Rassaerts, A. Schmidt, Planseeberichte für Pulvermetallurgie 14 (1966) 110–114.
[2] E. Gugel, P. Ettmayer, A. Schmidt, Berichte Deutsche Keramische Gesellschaft 45 (8) (1968) 395–402.
[3] J. Weiss, H.L. Lukas, J. Lorenz, G. Petzow, H. Krieg, CALPHAD 5 (2) (1981) 125–140.
[4] H.L. Lukas, J. Weiss, H. Krieg, E.-Th. Henig, G. Petzow, High Temp.–High Press. 14 (1982) 607–615.
[5] K.G. Nickel, M.J. Hoffmann, P. Greil, G. Petzow, Adv. Ceram. Mater. 3 (6) (1988) 557–562.
[6] H. Wada, M.-J. Wang, T.-Y. Tien, J. Am. Ceram. Soc. 71 (1988) 837–840.
[7] J. Weiss, H.L. Lukas, Mater. Sci. Forum 47 (1989) 43–57.
[8] A.K. Misra, J. Mater. Sci. 26 (1991) 6591–6598.
[9] A. Jha, J. Mater. Sci. 28 (1993) 3069–3079.
[10] U. Neidhardt, H. Schubert, E. Bischoff, G. Petzow, Key Eng. Mater. 89–91 (1994) 187–192.
[11] J. Bill, F. Aldinger, Adv. Mater. 7 (1995) 775–787.
[12] F. Aldinger, M. Weinmann, J. Bill, Pure Appl. Chem. 70 (1998) 439–448.
[13] J. Bill, F. Aldinger, Z. Metallkd. 87 (1996) 827–840.
[14] R. Riedel, H.-J. Kleebe, H. Schönfelder, F. Aldinger, Nature 374 (1995) 526–528.
[15] R. Riedel, G. Passing, H. Schönfelder, R.J. Brook, Nature 355 (1992) 714–716.
[16] H.-J. Kleebe, D. Suttor, H. Müller, G. Ziegler, J. Am. Ceram. Soc. 81 (1998) 2971–2977.
[17] N. Saunders, P. Miodownik, CALPHAD (Calculation of Phase Diagrams): A Comprehensive Guide, in: R.W. Cahn (Ed.), Materials Series, Vol. 1, Pergamon, Oxford, 1998.
[18] H.J. Seifert, F. Aldinger, Thermodynamic calculations in the system Si–B–C–N–O, in: J. Bill, F. Wakai, F. Aldinger (Eds.), Precursor-Derived Ceramics, Wiley–VCH, Weinheim, 1999, pp. 165–174.
[19] J. Peng, H.J. Seifert, F. Aldinger, Thermal analysis of Si–C–N ceramics derived from polysilazanes, in: G. Müller (Ed.), Ceramics–

Processing, Reliability, Tribology and Wear, EUROMAT 99, Vol. 12, Wiley–VCH, 2000, pp. 120–126.
[20] H.J. Seifert, J. Peng, F. Aldinger, Die Konstitution von Si–B–C–N Keramiken, in: J. Heinrich, G. Ziegler, W. Hermel, H. Riedel (Eds.), Keramik/Simulation Keramik, Werkstoffwoche '98, 12–15 Oct., München, Vol. VII, Wiley–VCH, Weinheim, 1999, pp. 339–343.
[21] H.L. Lukas, S.G. Fries, J. Phase Equilibria 13 (1992) 532–541.
[22] B. Sundman, B. Jansson, J.-O. Anderson, Calphad 9 (1985) 153–190.
[23] J. Gröbner, H.L. Lukas, F. Aldinger, Calphad 20 (1996) 247–254.
[24] M. Hillert, S. Jonsson, B. Sundman, Z. Metallkd. 83 (1992) 648–654.
[25] A. Dinsdale, Calphad 15 (1991) 317–425.
[26] Scientific Group Thermodata Europe, Grenoble Campus, 1001 Avenue Centrale, BP66, F-38402 Saint Martin D'Heres, France, http://www.sgte.org
[27] J.-J. Liang, L. Topor, A. Navrotsky, A. Mitomo, J. Mater. Res. 14 (1999) 1959–1968.
[28] R. Riedel, A. Greiner, G. Miehe, W. Dressler, H. Fuess, J. Bill, Angew. Chem. 109 (1997) 657–660.
[29] P.H. Fang, J. Mater. Sci. Lett. 14 (1995) 536–538.
[30] H. Kleykamp, Ber. Bunsenges. Phys. Chem. 102 (1998) 1231–1234.
[31] P.A.G. O'Hare, I. Tomaszkiewicz, C.M. Beck II, H.J. Seifert, J. Chem. Thermodyn. 31 (1999) 303–322.
[32] J. Seitz, Polymer-Pyrolyse-Keramik auf Si/C/N-Basis, University of Stuttgart, Germany, 1996, Ph.D. Thesis.
[33] J. Seitz, J. Bill, J. Mater. Sci. Lett. 15 (1996) 391–393.
[34] H.J. Seifert, Z. Metallkd. 90 (1999) 1016–1024.
[35] H.L. Lukas, E.-Th. Henig, G. Petzow, Z. Metallkd. 77 (1986) 360–367.
[36] H.J. Seifert, H.L. Lukas, F. Aldinger, Ber. Bunsenges. Phys. Chem. 9 (1998) 1309–1313.
[37] J. Bill, J. Seitz, G. Thurn, J. Dürr, J. Canel, B.Z. Janos, A. Jalowiecki, D. Sautter, S. Schempp, H.P. Lamparter, J. Mayer, F. Aldinger, Phys. Stat. Sol. (a) 166 (1998) 269–296.